Journal of Marine Science and Technology

Volume 31 | Issue 2 Article 8

Three-dimensional higher-order compressive sensing for raypath separation in an acoustic waveguide

Fengyan Zhong
The Laboratory of Image Science and Technology, Southeast University, Nanjing 210096, China,
230198825@seu.edu.cn

Recommended Citation

Zhong, Fengyan (2023) "Three-dimensional higher-order compressive sensing for raypath separation in an acoustic waveguide," *Journal of Marine Science and Technology*: Vol. 31: Iss. 2, Article 8.
DOI: 10.51400/2709-6998.2694
Available at: https://jmstt.ntou.edu.tw/journal/vol31/iss2/8

RESEARCH ARTICLE

Three-dimensional Higher-order Compressive Sensing for Raypath Separation in an Acoustic Waveguide

Fengyan Zhong

The Laboratory of Image Science and Technology, Southeast University, Nanjing, 210096, China

Abstract

In an acoustic waveguide, the separation of multiple raypaths, especially close raypaths, is a challenging task in the presence of colored noise due to interference in the acoustic field. In this paper, a three-dimensional higher-order compressive sensing method for raypath separation is proposed. The method is applied on an array-to-array experimental configuration where both emitter and reception arrays are used. With the array-to-array configuration, the raypaths are characterized by three parameters including arrival direction, departure direction, and arrival time. Furthermore, the performance of the proposed algorithm is illustrated by simulations and experiments. The numerical results based on simulation illustrate that the proposed method reduces the computational complexity compared to the three-dimensional higher-order raypath separation algorithm, while it achieves the advantage of noise suppression. Moreover, the experimental results validate the detection ability of the proposed algorithm for separating close raypaths.

Keywords: Acoustic waveguide, Array-to-array configuration, Compressive sensing, Higher-order statistics

1. Introduction

In shallow-water waveguides, acoustic rays travel in multiple paths because of reflection at the boundaries of the water column and refraction in the water column. This multipath propagation property is extensively used in certain scientific problems, such as underwater source localization [1], underwater vehicle communication [2], and ocean acoustic tomography [3]. The use of multipath propagation can provide more useful information in these problems. However, it is impossible to access the information without eliminating the interference among raypaths produced by multipath propagation.

Many subspace-based algorithms have been developed for separating raypaths. With these algorithms, the separation of raypaths is achieved by maximizing a function derived based on the orthogonality of signal and noise subspaces. Multiple signal classification (MUSIC) [4] is one of most popular algorithms for separating raypaths. In particular, in the context of shallow-water ocean acoustic tomography, a group of high-resolution algorithms [5–8] were presented to separate fully correlated and even coherent raypaths to improve the low-resolution performance of the MUSIC algorithm. Generally, these high-resolution methods are performed in a poin[1]t-to-array configuration, which consists of an emitter and a vertical reception array. With the configuration, the eigenrays are characterized by two parameters: direction of arrival (DOA) and time of arrival (TOA). Thus, these methods detect the raypaths in a plan of DOA and TOA. However, the source separation performance of these methods drops sharply if two distinct arrivals that correspond to raypaths almost simultaneously arrive on the reception array and their receive angles are similar. It is a frequently encountered circumstance that the

Received 20 September 2022; revised 14 March 2023; accepted 1 June 2023.
Available online 30 June 2023
E-mail address: 230198825@seu.edu.cn.

https://doi.org/10.51400/2709-6998.2694

different arrivals are extremely close in angle and arrival time due to the sound-speed changes [9] in the waveguide. In such cases, the high-resolution approaches presented previously are not always sufficient to detect these close wave arrivals.

To identify close acoustic rays, Roux et al. [9] used an array-to-array configuration and presented a double beamforming algorithm. The array-to-array configuration is composed of an emitter array and a reception array. With this configuration, the direction of departure (DOD) is used as an additional discrimination parameter to identify raypaths. The double beamforming algorithm is applied to both arrays simultaneously and is capable of separating close raypaths in a three-dimensional domain (they are the DOA domain, TOA domain, and DOD domain). However, the beamforming-like method suffers from low-resolution performance because of the limited size of the two vertical source-receiver arrays. To overcome this drawback, Roux et al. [10] presented a double Capon algorithm and a double MUSICAL algorithm, which are considered extensions of the Capon and MUSIC algorithms, respectively, to an array-to-array configuration and achieved higher resolution performance than double beamforming. Recently, Jiang et al. [11] proposed a three-dimensional higher-order algorithm to improve the robustness to colored noise, which is an extension of a higher-order algorithm [6] to an array-to-array configuration. It inherits the advantage of high-order cumulants to suppress colored noise. However, it is confronted with significant computation time. Despite the use of a moderately sized array, the three-dimensional raypath separation method still takes many hours to separate arrivals that arrive in close proximity.

Methods of separating raypaths different from the subspace-based algorithms were proposed. These methods are based on compressive sensing (CS) and utilize the inherent sparse structure of underlying signals. Raypath separation is converted into a linear predetermined system with a sparsity constraint. Certain parameters, such as DOA and TOA, are estimated by solving the linear predetermined system. For the application of CS in underwater acoustics, Song et al. [1] applied CS to underwater acoustic source localization, and they finally demonstrated superior source localization performance, including superresolution capabilities and robustness against model mismatch. Li et al. [12] proposed a CS-based DOA estimation algorithm for underwater wideband signals. The experimental results illustrated the reliability and practicability of the proposed algorithm. Xenakia and Gerstoft [13] developed compressive beamforming for source localization, which exhibits superior performance compared to conventional algorithms in certain challenging conditions, such as coherent arrivals and single-snapshot data. A successive study on the performance of CS with single and multiple snapshots was presented by Xenakia and Gerstoft [14]. Shuang Li et al. [15] proposed a CS-based DOA estimation method for decorrelated signals by using the sparse presentation of higher-order statistics of sources. It utilizes the property that non-Gaussian information is conveyed by higher-order cumulants (orders greater than two) in non-Gaussian processes. The simulation results show that the algorithm is robust to spatially colored noise and allows the identification of more incoherent signals than receivers. However, in shallow-water waveguides, multiple wave arrivals stem from multipath propagation. Thus, these arrivals are coherent. As far as we know, there are no CS-based methods based on higher-order cumulants that focus on solving this problem.

In this paper, we propose a novel three-dimensional higher-order CS-based method to separate coherent raypaths. The proposed algorithm accounts for colored noise (colored noise is ubiquitous in ocean environments) and is performed in an array-to-array configuration. In addition, the performance of the proposed method is illustrated based on simulations and experiments. In addition, it is also compared with several existing raypath separation algorithms.

The remainder of this paper is structured as follows. In Sec. 2, we review the signal model for array-to-array configurations and then describe a three-dimensional higher-order CS-based algorithm. In Sec. 3, (1) simulation results are provided to illustrate the performance of separating close raypaths, (2) the robustness to noise is illustrated by several sets of synthetic data, and (3) the results with different sizes of the arrays are shown to elucidate the computational complexity of the proposed algorithm. In Sec. 4, (1) the noise suppression performance of the algorithm is evaluated by real data obtained from a small-scale experiment, and (2) the algorithm is applied to a section of sea trial data collected from a shallow-water propagation experiment. In Sec. 5, we conclude this paper and provide the future direction of research.

2. The three-dimensional higher-order compressive sensing algorithm for raypath separation

2.1. Signal model

The P raypaths propagate in an array-to-array configuration composed of an emitter array (N sources) and a reception array (M sensors). The P raypaths

at the frequency ν produced by the n^{th} source and received on the m^{th} receiver are modeled as [10]

$$x_{m,n,\nu} = s_\nu \sum_{p=1}^{P} a_p e^{\Phi_p} + b_{m,n,\nu} \tag{1}$$

where the source spectrum s_ν is assumed to be known, the additive noise $b_{m,n,\nu}$ is modeled as spatially uncorrelated. For the raypath p, a_p denotes the amplitude, ϕ_p denotes the delay between the m^{th} sensor and the n^{th} source.

The delay ϕ_p is written as

$$\phi_p = -j2\pi\nu\left(T_p + (m-m_{ref})\tau\left(\theta_p^r\right) + (n-n_{ref})\tau\left(\theta_p^e\right)\right) \tag{2}$$

with

$$\tau\left(\theta_p^r\right) = \Delta_r \sin\left(\theta_p^r\right)/c,$$
$$\tau\left(\theta_p^e\right) = \Delta_e \sin\left(\theta_p^e\right)/c.$$

where Δ_r and Δ_e denote the inter-sensor distance and the inter-source distance respectively. θ_p^r and θ_p^e denote the arrival angle on the reception array and the emitter angle on the emitter array, respectively.

The reference source and reference receiver are denoted by n_{ref} and by m_{ref}, respectively, where $n_{ref} = (N+1)/2$ and $m_{ref} = (M+1)/2$. T_p denotes the propagation time between the reference source and the reference receiver. c denotes the speed of wave propagation.

2.2. Data model

Based on the signal model built in Eq. (1), for all N sources, M receivers, and F frequencies of wideband signal used in the algorithm, each signal received in the array-to-array configuration is a data cube. The data model is constructed by concatenating the elements of the data cube into a long vector. The construction process consists of three steps.

First, the elements corresponding to the source n^{th} at the frequency ν on all the M elements of the receiver array are concatenated into the vector

$$\mathbf{x}_{n,\nu} = [x_{1,n,\nu} \ldots x_{M,n,\nu}]^+ \tag{3}$$

where $+$ means transpose.

Then, the elements corresponding to both the N source and the M sensors are further concatenated into the vector

$$\mathbf{x}_\nu = [\mathbf{x}_{1,\nu} \ldots \mathbf{x}_{n,\nu}]^+ \tag{4}$$

Finally, the long vector $\mathbf{x}$ considering all the F frequencies is given by

$$\mathbf{X} = [\mathbf{x}_{\nu_1} \ldots \mathbf{x}_{\nu_F}]^+ \tag{5}$$

Similarly, the steering vector $\mathbf{d}(\theta_p^r, \theta_p^e, T_p)$ and the additive noise vector $\mathbf{b}$ are obtained by concatenating the steering vector and the observed noise vector at each frequency ν into long vectors, respectively. Thus, the received signal in the frequency domain is written as

$$\mathbf{X} = \sum_{p=1}^{p} a_p \mathbf{d}\left(\theta_p^r, \theta_p^e, T_p\right) + \mathbf{b} = \mathbf{D}(\boldsymbol{\theta}^r, \boldsymbol{\theta}^e, \mathbf{T})\mathbf{a} + \mathbf{b} \tag{6}$$

where $\mathbf{a}$ is an $P \times 1$ vector of raypaths, $\boldsymbol{\theta}^r = [\theta_1^r, \theta_2^r, \cdots, \theta_P^r]^+$, $\boldsymbol{\theta}^e = [\theta_1^e, \theta_2^e, \cdots, \theta_P^e]^+$, $\mathbf{T}_p = [T_1, T_2, \cdots, T_P]^+$. The terms $\mathbf{X}$, $\mathbf{d}(\theta_p^r, \theta_p^e, T_p)$, and $\mathbf{b}$ are respectively expressed as

$\mathbf{X} = [\mathbf{x}_{\nu_1}, \mathbf{x}_{\nu_2}, \cdots, \mathbf{x}_{\nu_F}]^+$, $\mathbf{x}_\nu = [\mathbf{x}_{1,\nu}, \mathbf{x}_{2,\nu}, \cdots, \mathbf{x}_{N,\nu}]^+$ $(\nu = \nu_1, \nu_2, \cdots, \nu_F)$, with

$\mathbf{x}_{n,\nu} = [x_{1,n,\nu}, x_{2,n,\nu}, \cdots, x_{M,n,\nu}]^+$ $(n = 1, 2, \cdots, N)$.

$\mathbf{d}(\theta_p^r, \theta_p^e, T_p) = [\mathbf{d}_{\nu_1}(\boldsymbol{\theta}_p^e, \boldsymbol{\theta}_p^r, T_p), \mathbf{d}_{\nu_2}(\boldsymbol{\theta}_p^e, \boldsymbol{\theta}_p^r, T_p), \cdots, \mathbf{d}_{\nu_F}\left(\boldsymbol{\theta}_p^e, \boldsymbol{\theta}_p^r, T_p\right)\Big]^+$

with $\mathbf{d}_{\nu_i}(\boldsymbol{\theta}_p^e, \boldsymbol{\theta}_p^r, T_p) = [s_{\nu_i} e^{-j2\pi\nu_i(T_p + (1-n_0)\tau(\theta_p^e))}$

$\mathbf{d}\left(\boldsymbol{\theta}_p^r\right)_{\nu_i}, \cdots, s_{\nu_i} e^{-j2\pi\nu_i\left(T_p + (N-n_0)\tau\left(\theta_p^e\right)\right)} \mathbf{d}\left(\boldsymbol{\theta}_p^r\right)_{\nu_i}\Big]^+$

and $\mathbf{d}(\boldsymbol{\theta}_p^r)_{\nu_i} = [e^{-j2\pi\nu_i(1-m_0)\tau(\theta_p^r)}, \cdots, e^{-j2\pi\nu_i(M-m_0)\tau(\theta_p^r)}]^+$.

$\mathbf{b} = [\mathbf{b}_{\nu_1}, \mathbf{b}_{\nu_2}, \cdots, \mathbf{b}_{\nu_F}]^+$, with $\mathbf{b}_\nu = [\mathbf{b}_{1,\nu}, \mathbf{b}_{2,\nu}, \cdots, \mathbf{b}_{N,\nu}]^+ (\nu = \nu_1, \nu_2, \cdots, \nu_F)$, and $\mathbf{b}_{n,\nu} = [b_{1,n,\nu}, b_{2,n,\nu}, \cdots, b_{M,n,\nu}]^+ (n = 1, 2, \cdots, N)$.

2.3. Principle of the algorithm

Based on the data model in Eq. (6), the trispectrum matrix is computed directly. However, in a multipath propagation environment, the raypaths are fully correlated or coherent. The coherence inevitably leads to rank deficiency in the trispectrum matrix and the resolution performance thus degrades. To improve the separation resolution, a joint spatial-frequency smoothing strategy [6,7] is used as a preprocessing step. All recurrences $\mathbf{x}_{i,j,k}$ produced by spatial-frequency smoothing are used to compute the expected broadband trispectrum matrix. The smoothing trispectrum matrix is then defined as the average of the $K_e \times K_r \times K_f$ trispectrum matrices. It is expressed as Eq. (7) and the smoothing technique for the cumulants is shown in Fig. 1.

$$\widehat{\mathbf{C}}=\frac{1}{K_eK_rK_f}\sum_{k=1}^{K_f}\sum_{j=1}^{K_e}\sum_{i=1}^{K_r}\mathbf{C}_{i,j,k}$$
$$=\frac{1}{K_eK_rK_f}\sum_{k=1}^{K_f}\sum_{j=1}^{K_e}\sum_{i=1}^{K_r}E\left\{\left(\mathbf{X}_{i,j,k}\otimes\mathbf{X}_{i,j,k}^{*}\right)\left(\mathbf{X}_{i,j,k}\otimes\mathbf{X}_{i,j,k}^{*}\right)^{H}\right\}$$
$$-E\left\{\left(\mathbf{X}_{i,j,k}\otimes\mathbf{X}_{i,j,k}^{*}\right)\right\}E\left\{\left(\mathbf{X}_{i,j,k}\otimes\mathbf{X}_{i,j,k}^{*}\right)^{H}\right\}$$
$$-E\left\{\left(\mathbf{X}_{i,j,k}\mathbf{X}_{i,j,k}^{H}\right)\right\}\otimes E\left\{\left(\mathbf{X}_{i,j,k}\mathbf{X}_{i,j,k}^{H}\right)^{*}\right\} \tag{7}$$

where $\mathbf{X}_{i,j,k}$ denotes the received signal corresponding to the i^{th} subarray of the reception array, the j^{th} subarray of the emitter array, and the k^{th} subband of the band. K_e and K_r are the spatial smoothing factors on the emitter and reception arrays, respectively, and K_f is the frequency smoothing factor. The symbols * and ^{H} mean conjugated and transpose conjugated, respectively.

Here, we rewrite the trispectrum matrix as

$$\widehat{\mathbf{C}}=\mathbf{B}\mathbf{C}_s\mathbf{B}^H \tag{8}$$

where the size of $\widehat{\mathbf{C}}$ is $(M\times N\times F)^2\times(M\times N\times F)^2$. $\mathbf{C}_s\in\mathbb{C}^{P\times P}$ is the trispectrum matrix related to raypaths, it is a diagonal matrix with diagonal being $\mathbf{a}$, $\mathbf{B}=[\mathbf{b}_1,\mathbf{b}_2,\ldots,\mathbf{b}_P]\in\mathbb{C}^{(M\times N\times F)^2\times P}$ is the extended steering matrix that corresponds to P raypaths with $\mathbf{b}_k=\mathbf{d}_k\otimes\mathbf{d}_k^*$. We set $K=M\times N\times F$.

To reduce computational complexity, dimension reduction preprocessing is introduced to eliminate the redundant information in the matrices $\mathbf{B}$ and $\widehat{\mathbf{C}}$. The preprocessing consists of the following two steps:

The first step is to remove the redundant items in $\mathbf{B}$. To do this, a $K^2\times(2K-1)$ transformation matrix $\mathbf{H}$ is constructed by using the construction method proposed in Ref. [16], as is shown in Eq. (9),

$$\mathbf{H}=\left[\mathbf{H}_1^T,\mathbf{H}_2^T,\ldots,\mathbf{H}_K^T\right]^T \tag{9}$$

with

$$\mathbf{H}_m=\begin{cases}\left[\mathbf{0}_{K\times(K-1)}\quad\mathbf{I}_K\right] & m=1\\ \left[\mathbf{0}_{K\times(K-1)}\quad\mathbf{I}_K\quad\mathbf{0}_{K\times(m-1)}\right] & 2\le m\le K-1\\ \left[\mathbf{I}_K\quad\mathbf{0}_{K\times(K-1)}\right] & m=K\end{cases} \tag{10}$$

where $\mathbf{I}_K$ is the $K\times K$ identity matrix, the symbol ^{T} means transposed. It is possible to produce a reduced-dimension $(2K-1)\times P$ steering matrix $\mathbf{F}$ by using the matrix $\mathbf{H}$, such that

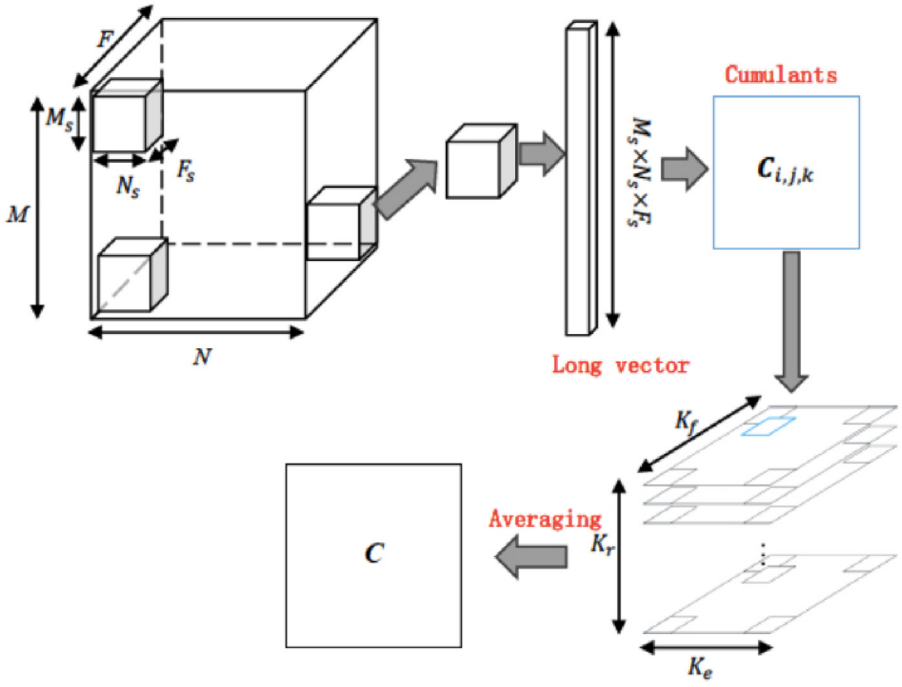

Fig. 1. The smoothing technique for the cumulants.

$$\mathbf{B} = \mathbf{HF} \tag{11}$$

Substituting Eq. (11) into Eq. (8), one obtains

$$\widehat{C} = (\mathbf{HF})\mathbf{C}_s(\mathbf{HF})^H \tag{12}$$

In the second step, by eliminating the redundant entries in the matrix $\widehat{\mathbf{C}}$, a dimension-reduced $(2K-1)\times(2K-1)$ trispectrum matrix $\widehat{\mathbf{C}}_4$ is obtained, which is given by

$$\begin{aligned}\widehat{\mathbf{C}}_4 &= \mathbf{G}^{-1}\mathbf{H}^T\widehat{\mathbf{C}}\mathbf{H}\mathbf{G}^{-1} = \mathbf{G}^{-1}\mathbf{H}^T(\mathbf{HF})\mathbf{C}_s(\mathbf{HF})^H\mathbf{H}\mathbf{G}^{-1}\\ &= \mathbf{F}\mathbf{C}_s\mathbf{F}^H\end{aligned} \tag{13}$$

where $\mathbf{G} = \mathbf{H}^T\mathbf{H} = \mathrm{diag}(1,2,\ldots,K-1,K,K-1,\ldots,1)$.

By concatenating the elements of the matrix $\widehat{\mathbf{C}}_4$ into a long vector, Eq. (13) is rewritten as

$$\mathbf{z} = \mathrm{vec}(\widehat{\mathbf{C}}_4) = \mathrm{vec}\left(\mathbf{F}\mathbf{C}_s\mathbf{F}^H\right) = (\mathbf{F}^* \odot \mathbf{F})\mathbf{a} = \mathbf{Q}\mathbf{a} \tag{14}$$

where the size of $\mathbf{z}$ is $(2K-1)^2\times 1$, the notation $\odot$ denotes the KR product, vec($\cdot$) denotes the vectorization operator that stacks the columns of a matrix, and the size of $\mathbf{Q}$ is $(2K-1)^2\times P$.

Based on the abovementioned preprocessing, the computational complexity is largely reduced because the scale of the problem in Eq. (14) is much less than that of the problem in Eq. (8), especially when the size of the array is increased.

Based on Eq. (14), the problem of raypath separation is formulated into a higher-order cumulant-based L_1 regularization optimization problem. For all raypaths, three sample sets are constructed, which represent their potential DODs A, their potential DOAs B, and their potential TOPs C. $A = \{\theta_1^e, \theta_2^e, \ldots, \theta_{d_e}^e\}$, $B = \{\theta_1^r, \theta_2^r, \ldots, \theta_{d_r}^r\}$, and $C = \{T_1, T_2, \ldots, T_{d_t}\}$. Then, the raypaths are identified in a three-dimensional grid of size $d_e \times d_r \times d_t$. Let $W = d_e \times d_r \times d_t$. We assume that the three-dimensional grid is dense enough that the theoretical position of raypaths is expected to be located on the grid or close to the grid.

Using the three-dimensional grid, Eq. (14) can be reformulated as

$$\mathbf{z} = \tilde{\mathbf{Q}}\mathbf{p}_N \tag{15}$$

where the $(2K-1)^2\times W$ matrix $\tilde{\mathbf{Q}}$ denotes the sensing matrix and the $W\times 1$ vector $\mathbf{p}_N$ is an unknown vector containing information about raypaths at all grid points. The $(i\times j\times k)$-th element of $\mathbf{p}_N$ is nonzero if a raypath p falls on the $(i\times j\times k)$-th grid point; otherwise, it equals zero. Thus, $\mathbf{p}_N$ is P-sparse in the case of $W \gg P$ because there are only P nonzero elements in $\mathbf{p}_N$. The CS framework asserts that the sparse signal $\mathbf{p}_N$ can be reconstructed accurately by solving a L_2 regularization optimization problem [13], and the solution is $\widehat{\mathbf{p}}_N$, as shown in Eq. (16),

$$\widehat{\mathbf{p}}_N = \underset{\mathbf{p}_N\in\mathbb{C}^W}{\mathrm{argmin}} \parallel \mathbf{z} - \tilde{\mathbf{Q}}\mathbf{p}_N\parallel_2^2 + \mu \parallel \mathbf{p}_N\parallel_2^2 \tag{16}$$

where $\|\cdot\|_2$ denotes the l_2-norm and the regularization parameter μ controls the l_2-norm term $\left\|\mathbf{z} - \tilde{\mathbf{Q}}\mathbf{p}_N\right\|_2^2$ between the solution's sparsity. This paper finds the solution via a reedy sparse approximation strategy rather than a second-order cone (SOC) programming framework. The reedy sparse approximation strategy is an important method for DOA estimation and has advantages such as low computational complexity, simplicity in implementation, and high robustness [17]. Based on Eq. (16), the raypath separation problem is finally formulated as the L_2-norm minimization problem (Eq. (16)). Parameters such as DODs, DOAs, and TOAs are estimated according to the solution $\widehat{\mathbf{p}}_N$.

3. Simulations

In this section, several simulations are provided to illustrate the performance of the proposed method. We define the signal-to-noise ratio (SNR) as the ratio of signal power and noise power in the frequency band of the signal. The smoothing-MUSICAL [5], double MUSICAL [10], and double-4s-MUSICAL [11] are taken as comparative algorithms. Both the double-4s-MUSICAL and the proposed algorithm are applied to an array-to-array configuration. The smoothing-MUSICAL is applied to a point-to-array configuration. In the point-to-array configuration, the point source is fixed at the center of the emitter array, and the reception array is the same as the one used in the array-to-array configuration.

3.1. Example with an array-to-array configuration composed of seven elements

This subsection provides an example to illustrate the detection performance of the proposed algorithm for close raypaths under noiseless circumstances. As an example of this situation, we assume that four acoustic rays propagate between the centers of the emitter array and the reception array in the waveguide. Both the emitter and reception arrays are composed of seven elements. The elements on the emitter array are regularly spaced in the water column between 82.5 and 97.5 m. The reception array is set between 42.5 and 57.5 m under the water. The centers of the emitter array and

reception array are set at 90 m and 50 m, respectively. The distance between the two adjacent elements of the arrays is 2.5 m. The horizontal distance between the two arrays is 1500 m. The acoustic sound speed is 1500 m/s in the waveguide, and the sampling frequency is 10,000 Hz. Fig. 2 shows the separation results of these algorithms. Seven frequency bins are used in this simulation, and their values range from 1.25 to 1.75 kHz. In Fig. 2, each spot represents the arrival of the raypath, and black crosses are added to mark the theoretical positions of the raypaths. The smoothing-MUSICAL separates raypaths in a plan of TOA and DOA, while the proposed algorithm, double MUSICAL, and double-4s-MUSICAL use DOA, DOD, and TOA to separate raypaths in three-dimensional space. The spots provided by the double-4s-MUSICAL are located at max-value/1.5. Both the proposed algorithm and double MUSICAL mark the spot at max-value/15.5. Four raypaths are clearly detected in Fig. 2(b), (c), and (d), whereas close arrivals are shown as a mixed point in Fig. 2(a). Table 1 shows the comparisons of the estimation errors for the proposed algorithm, double MUSICAL, and double-4s-MUSICAL. The proposed algorithm and double-4s-MUSICAL give similar errors, whereas the double MUSICAL produces relatively high errors.

3.2. *Quantified analysis of the performance*

Next, a quantified analysis is provided to verify the performance of the proposed method. For a

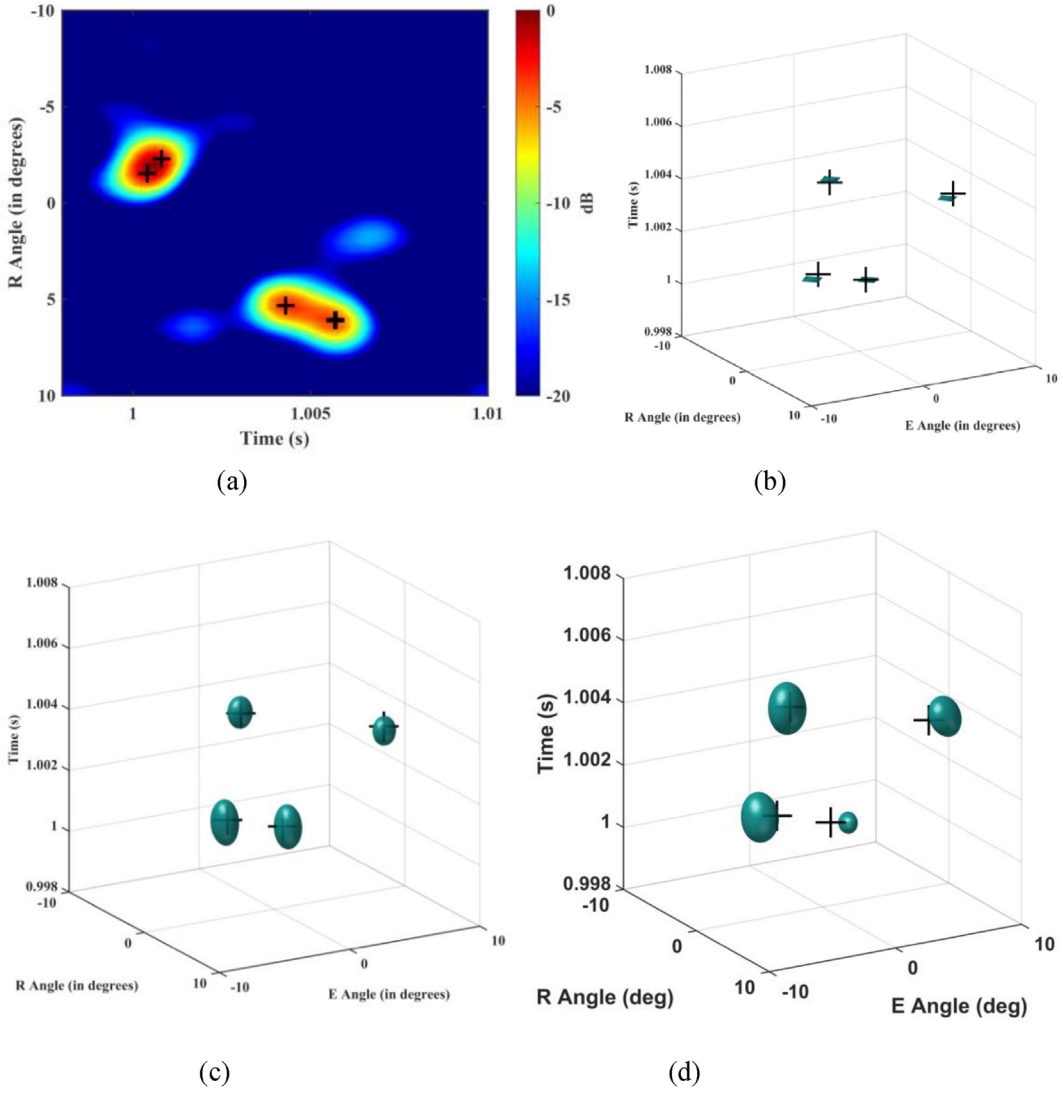

Fig. 2. Comparison of the results (four raypaths propagate between the centers of emitter and reception arrays). Black crosses are added to mark the theoretical positions of the raypaths. (a) Separation results using the smoothing-MUSICAL algorithm. (b) Separation results using the proposed algorithm. (c) Separation results using the double-4s-MUSICAL algorithm. (d) Separation results using the double MUSICAL algorithm.

Table 1. Error comparison in simulation.

	double-4s-MUSICAL	Proposed method	double MUSICAL
emission angle (°)	0.29	0.46	1.05
reception angle (°)	0.22	0.32	0.8
arrival time (us)	92	94	172

given method, the root-mean-square error (RMSE) is used to quantify the estimation error of the relevant parameters. The RMSE of the arrival time is defined as Eq. (17). The RMSEs of the reception and emission angles are similar to that of the arrival time,

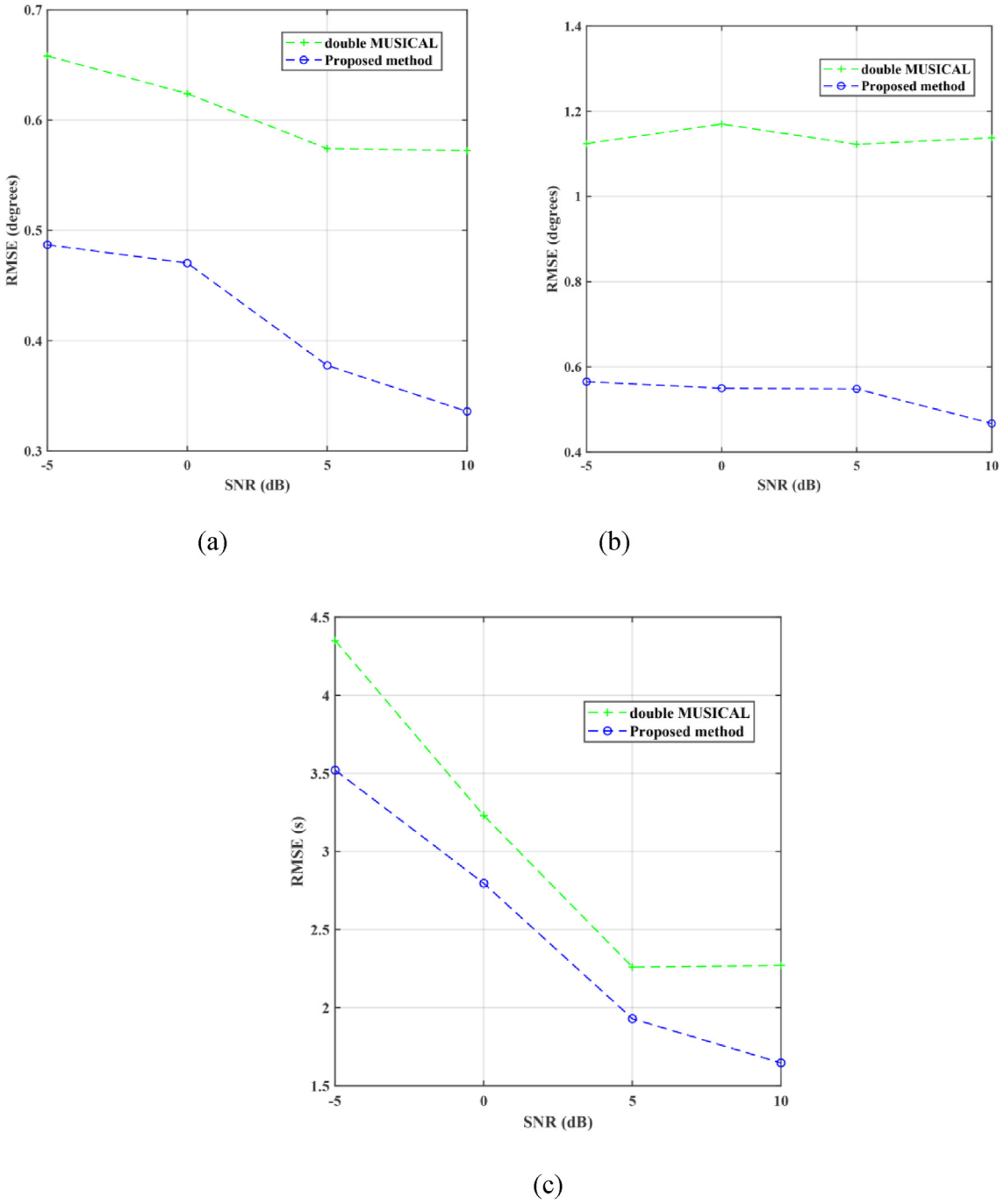

Fig. 3. The RMSEs comparison for the proposed algorithm and double MUSICAL algorithm, estimated by 10 realizations. (a) RMSE comparison of DOA estimation. (b) RMSE comparison of DOD estimation. (c) RMSE comparison of TOA estimation.

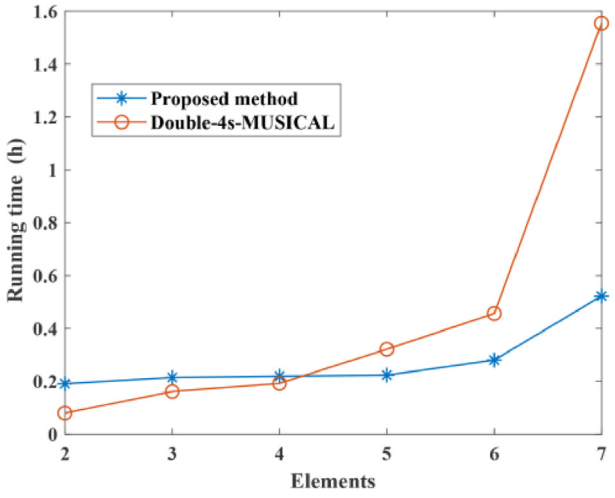

Fig. 4. Computation Time analysis as a function of N for the proposed algorithm and double-4s-MUSICAL algorithm.

$$RMSE_t = \sqrt{\frac{1}{KP}\sum_{k=1}^{K}\sum_{i=1}^{P}\left(\hat{t}_k^i - t^i\right)^2} \tag{17}$$

where $\hat{t}_k^i$ is the estimation of t^i for the i^{th} raypath in the k^{th} realization. K is the number of realizations, which is set as K = 10 in the following simulations. The other conditions are kept the same as in Fig. 2. Fig. 3 shows the RMSE comparison for DOA, DOD, and TOA estimations in the proposed method and double MUSICAL algorithm. It is clear in Fig. 3 that the proposed method is less sensitive to noise than the double MUSICAL algorithm.

3.3. Influence of the element on performance

Then, the computation time of the proposed algorithm with respect to the number of elements is investigated. Parameter settings are the same as in the previous section. The computation time is a function of the number of elements of the reception array. The number of elements of the emitter array is set as the same as the number of elements of the reception array, i.e., $M = N$. Fig. 4 illustrates that using the proposed algorithm requires much less computation time than the double-4s-MUSICAL, especially when a large number of elements are used, although both take advantage of the suppression ability of higher-order cumulants and the array-to-array configuration. Thus, one of the great advantages of the proposed algorithm is that it can save significant computation time, which has great value for applications in systems with computation time requirements.

4. Experiments

In this section, to further illustrate the performance of the proposed algorithm, small-scale experiments and shallow-water propagation experiments are discussed. The small-scale experiment focuses on the robustness performance of the proposed algorithm. We take the double MUSICAL [10] and smoothing-MUSICAL [5] as comparative algorithms in the small-scale experiment. The shallow-water propagation experiment shows the ability to separate close acoustic rays. Double-4s-MUSICAL [11], double MUSICAL [10], and 4s-smoothing-MUSICAL [6] are used for comparison in the shallow-water propagation experiment.

4.1. Small-scale experiment

The small-scale experiment was developed by P. Roux [18] in a laboratory ultrasonic tank. This tank is 1 m long and 55 mm deep. Its bottom is covered by a steel bar, which facilitates the optimal reflection of sound waves at this interface. Two coplanar arrays are placed at a distance of 1 m, called the emitter array and reception array. Both of them are composed of 64 transducers, and the distance between the transducers is 0.75 mm. The emitter array emits an ultrasonic signal with a wavelength of 1.5 mm and a broadband frequency of 0.5 MHz, which has a center frequency of 1 MHz. The sampling frequency is 10 MHz. The double MUSICAL, smoothing-MUSICAL, and the proposed algorithm are applied to the same set of real data obtained by this small-scale experiment, and the separation results are shown in Fig. 5(a) and (b), and (c). SNR is fixed to 20 dB. The number of frequencies used is 12, and the frequency bin value is from 757,575 to 1,590,909 Hz. Each spot indicates the arrival of a raypath. The black crosses are added to show the theoretical positions of raypaths, as shown in Fig. 5. The smoothing-MUSICAL is applied to a point-to-array configuration. The receive subarray is composed of 7 elements with a spacing of 1.5 mm, covering the water column from 19.5 to 28.5 mm. Both the emitter and reference transducers are set at a depth of 24 mm. With this configuration, the smoothing-MUSICAL gives a two-dimensional separation result in a plan of TOA and DOA, as shown in Fig. 5(b). The other algorithms are applied to an array-to-array configuration. Each array in the configuration is composed of 7 transducers. Both the emitter subarray and reception subarray cover the water column from the position at 19.5 mm to the position at 28.5 mm. By taking

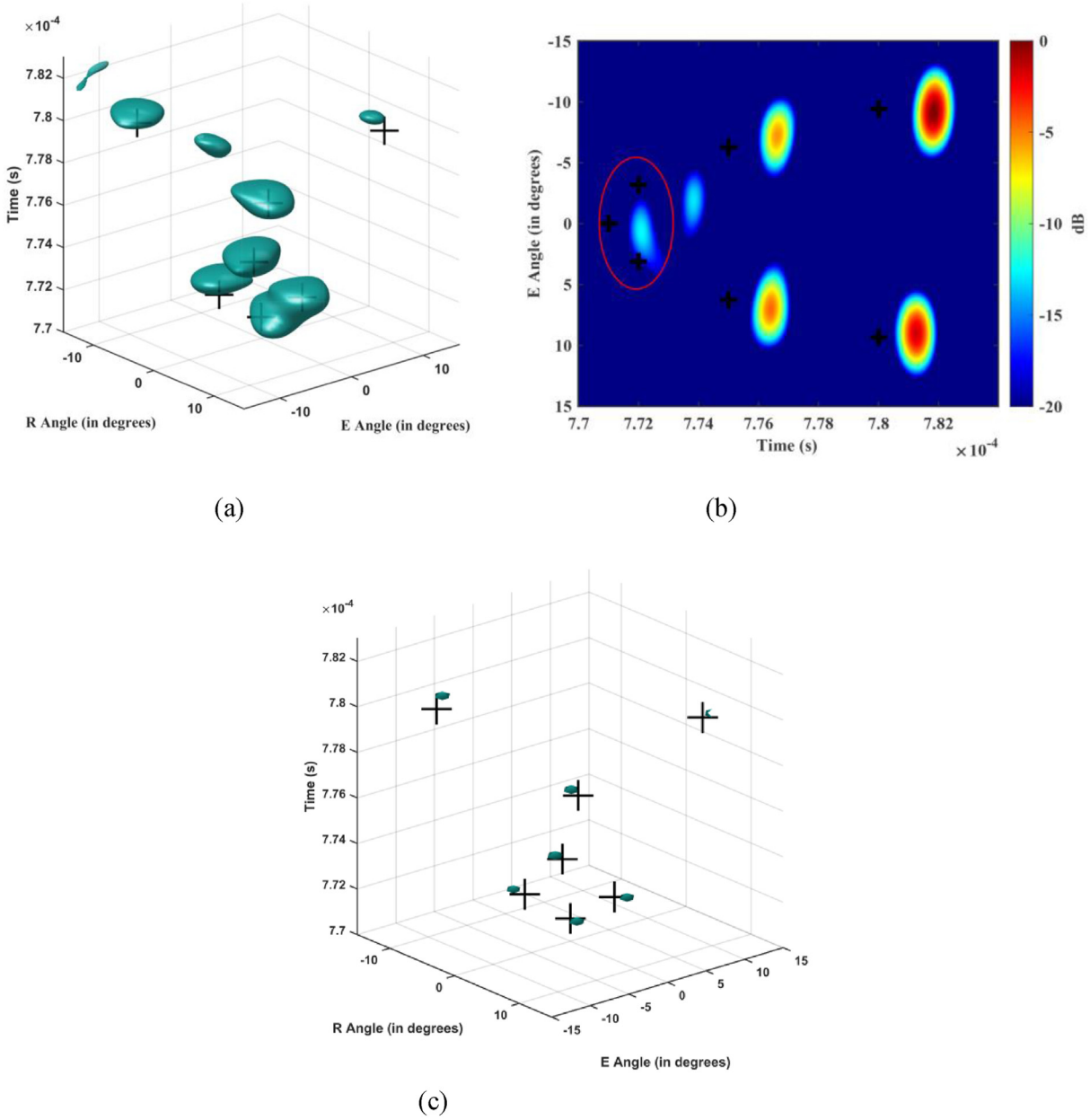

Fig. 5. Results comparison in the small-scale experiment. Black crosses are added to indicate the theoretical positions of raypaths. (a) Separation results using the double MUSICAL algorithm. (b) Separation results using the smoothing-MUSICAL algorithm. (c) Separation results using the proposed algorithm.

advantage of the array-to-array configuration, a three-dimensional separation is provided, as shown in Fig. 5(a) and (c). Spots represent the estimated position of the raypath. The spots provided by the double MUSICAL and the proposed algorithm are located at max-value/1.3 and max-value/25, respectively.

Table 2. Error comparison in small-scale experiment.

	Double MUSICAL	Proposed method
emission angle (°)	1.15	0.62
reception angle (°)	1.0	0.72
arrival time (ns)	367	302

Comparing Fig. 5(a) and (c), the proposed algorithm shows a relatively smaller spot for each raypath than the double MUSICAL and presents smaller estimation errors, as shown in Table 2. In addition, all arrivals are clearly detected in Fig. 5(c). However, in Fig. 5(a), the first and third raypaths fail to be totally separated because the use of the smoothing technique leads to a

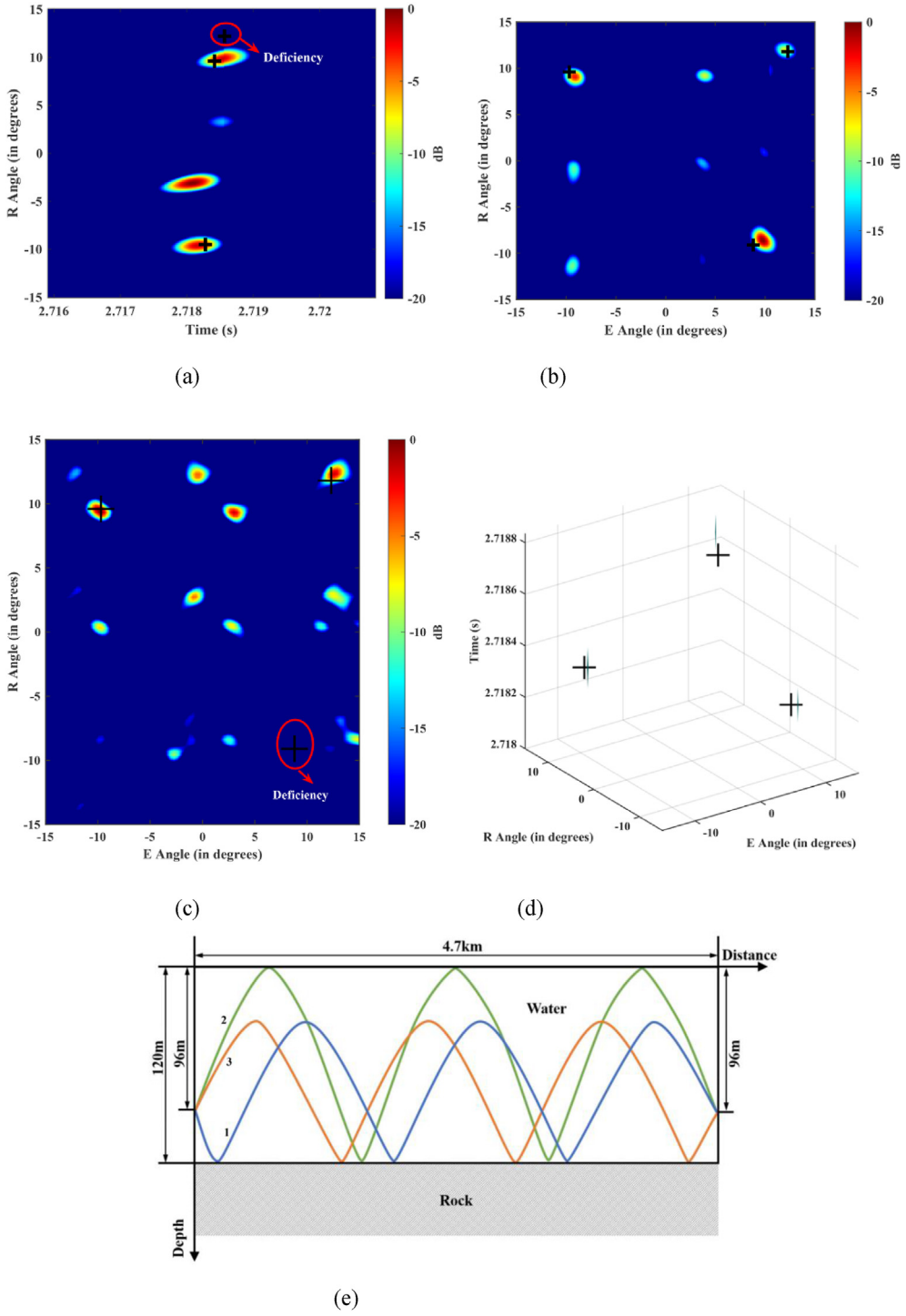

Fig. 6. Results comparison with the data collected from shallow-water propagation experiment. Black crosses are added to indicate the theoretical positions of raypaths. (a) Separation results with the 4s-smoothing-MUSICAL algorithm. (b) Separation results with the double-4s-MUSICAL algorithm. (c) Separation results with the double MUSICAL algorithm. (d) Separation results with the proposed algorithm. (e) Propagation path of three acoustic waves to be separated in shallow-water propagation experiment.

reduction in the array aperture and bandwidth (these raypaths are referred to successively from bottom to top and from left to right). In Fig. 5(b), the smoothing-MUSICAL enables the separation of the last four raypaths. However, it presents one mixed spot for the first three arrivals because the propagation times of these arrivals are extremely close.

Table 3. Error comparison in small-scale experiment.

	double-4s-MUSICAL	Proposed method
emission angle (°)	0.51	0.29
reception angle (°)	0.76	0.36
arrival time (ns)	\	68.04

4.2. Shallow-water propagation experiment

The shallow-water propagation experiment was conducted in July 2005 north of Elba Island, Italy [9]. The configuration of this experiment is similar to that of the small-scale experiment, but the former spans much more water than the latter. Detailed information about the shallow-water propagation experiment can be found in Sec. II in Ref. [9]. In this experiment, a vertical array composed of five hydrophones is taken as a reception, covering the water column from the position at 88 m to the position at 96 m with a spacing of 2 m. A vertical array composed of five equally spaced transducers is taken as an emission, spanning 11.144 m in a 123 m water column at a water depth of 123 m. The distance between the two adjacent transducers is 2.786 m. Both the reference hydrophone and the reference transducer are set at 96 m at a water depth of 123 m. The source signal with a 1 kHz frequency bandwidth has a central frequency of 3.2 KHz. The 11 frequency bins of the signal are used, and their value ranges from 2.2 KHz to 4.2 KHz. Sixty taps of the broadband time-domain signal with a sampling frequency of 12 kHz are used in this experiment. The maximum SNR of the noise field is approximately 40 dB.

Fig. 6(e) displays the propagation trajectories of three special acoustic waves between the centers of the source and receive arrays. Both the centers of the source and receive arrays have a depth of 96 m. Among the three raypaths, raypath 2 is a surface-reflected ray, whereas raypaths 1 and 3 are refracted rays. Due to the sound speed variation in the water [9], the three acoustic rays arrived at the center of the reception array in similar times. In addition, raypaths 1 and 2 have close DOAs, while raypaths 2 and 3 have close DODs. Fig. 6(a), (b), 6(c), and 6(d) show the separation results of separating the three raypaths in Fig. 6(e) using the 4s-smoothing-MUSICAL, the double-4s-MUSICAL, the double MUSICAL, and the proposed algorithm, respectively. Each spot corresponds to the estimated position of the raypath. The spot provided by the proposed algorithm is located at max-value/30. As shown in Fig. 6(b) and (d), both the double-4s-MUSICAL algorithm and our algorithm successfully identify the three raypaths. The comparisons of the results in Table 3 also illustrate the similar performance of the proposed method and double-4s-MUSICAL algorithm. In Fig. 6(a), there is a deficient raypath, indicating that the third raypath is not detected by the four-smoothing-MUSICAL algorithm in the TOA and DOD plans. This is because the second raypath and the third raypath have close DOAs and TOAs. The double MUSICAL algorithm separates the two raypaths well in the domain of DOD and DOA by making use of the advantage of the array-to-array configuration. However, a deficient raypath is also presented due to the small number of elements used.

5. Conclusion

In this paper, a three-dimensional high-order compressive sensing algorithm is proposed to separate coherent raypaths in a shallow-water waveguide. Our method is applied to the array-to-array configuration and is less sensitive to noise. Compared to existing algorithms that are applied on a point-to-array configuration, the proposed algorithm achieves higher resolution when separating close raypaths. Moreover, the proposed method has an obvious advantage in computational complexity over the three-dimensional higher-order subspace-based algorithm. In the future, a multidimensional gridless compressive sensing version of the proposed algorithm will be studied to obtain a more accurate separation when the basis mismatch effect exists.

Conflict of interest

The authors declare that they have no known competing financial interests or personal relationships that could have appeared to influence the work reported in this paper.

Acknowledgments

This research was supported by the National Natural Science Foundation of China (No: 61871124 and 61876037), with funding from the China Ship Development and Design Center (No. JJ-2021-702-05), and the National Key Laboratory of Science and Technology on Underwater Acoustic Antagonizing (No: 2021-JCJQ-LB-033-09).

References

[1] Song HY, Yang CY, Wang KJ. Robust super-resolution approach to source localization in ocean waveguide using sparsity constraint. J Mar Sci Technol 2019;27(1):17−27.
[2] Uysal E, Ylmaz S, Kuzlu M. Digital acoustic modem design for narrowband underwater vehicle communications. J Mar Sci Technol 2018;26(4):594−603.

[3] Munk W, Wunsch C. Ocean acoustic tomography: A scheme for large scale monitoring, Deep Sea Research Part A. Oceanographic Research Papers 1979;26(2):123−216.
[4] Schmidt R. Multiple emitter location and signal parameter estimation. IEEE Trans Antenn Propag 1986;34(3):276−80.
[5] Jiang L, Aulanier F, Le Touźe G, Nicolas B, Mars JI. Raypath separation with high resolution processing. In: OCEANS 2011 IEEESpain. IEEE; 2011. p. 1−5.
[6] Jiang L, Hong Y, Roux P, Wu J, Shu H. Active wideband higherorder raypath separation in multipath environment. J Acoust Soc Am 2017;141(1):EL38−44.
[7] Jiang L, Roux P, Mars JI. Raypath separation with a high-resolution algorithm in a shallow-water waveguide. IEEE J Ocean Eng 2017;43(1):119−30.
[8] Jiang L, Song W, Zhang Z, Yang C, Wang S, Roux P. Fast raypath separation based on low-rank matrix approximation in a shallow-water waveguide. J Acoust Soc Am 2018;143(4):EL271−7.
[9] Roux P, Cornuelle BD, Kuperman W, Hodgkiss W. The structure of raylike arrivals in a shallow-water waveguide. J Acoust Soc Am 2008;124(6):3430−9.
[10] Le Touźe G, Nicolas B, Mars JI, Roux P, Oudompheng B. Doublecapon and double-musical for arrival separation and observable estimation in an acoustic waveguide. EURASIP J Appl Signal Process 2017;143(1):EL271−8.
[11] Jiang L, Zhang Z, Roux P. Three dimensional higher-order raypath separation in a shallow-water waveguide. 2021. arXiv:2103.14206. URL, https://arxiv.org/abs/2103.14206.
[12] Li Z, Li S, Jia J, Ju D. Doa estimation of underwater wideband signals based on improved omp method. In: Oceans 2019 - marseille; 2019. p. 1−6.
[13] Xenaki A, Gerstoft P, Mosegaard K. Compressive beamforming. J Acoust Soc Am 2014;136(1):260−71.
[14] Gerstoft P, Xenaki A, Mecklenbr̈auker CF, Zochmann E. Multiple snapshot compressive beamforming. In: 2015 49th asilomar conference on signals, Systems and Computers; 2015. p. 1774−8.
[15] Li S, Jiang X, He W, Wang Y. Direction of arrival estimation via sparse representation of fourth order statistics. In: 2013 IEEE international conference on signal processing, communication and computing (ICSPCC 2013); 2013. p. 1−4.
[16] Ma WK, Hsieh TH, Chi CY. Doa estimation of quasi-stationary signals with less sensors than sources and unknown spatial noise covariance: A khatri{rao subspace approach. IEEE Trans Signal Process 2010;58(4):2168−80.
[17] Donoho DL, Tsaig Y, Drori I, Starck JL. Sparse solution of underdetermined systems of linear equations by stagewise orthogonal matching pursuit. IEEE Trans Inf Theor 2012; 58(2):1094−121.
[18] Roux P, Kuperman WA, Hodgkiss WS, Song HC, Akal T, Stevenson M. A nonreciprocal implementation of time reversal in the ocean. J Acoust Soc Am 2004;116(2): 1009−15.